Optics Letters

Design of a large field-of-view see-through near to eye display with two geometrical waveguides

Jianming Yang,[1,2,*] Patrice Twardowski,[1] Philippe Gérard,[1] and Joël Fontaine[1]

[1]ICube UMR-7357, CNRS, University of Strasbourg, INSA, Strasbourg-Illkirch, France
[2]Changchun Institute of Optics, Fine Mechanics and Physics, Chinese Academy of Sciences, Changchun, Jilin 130033, China
*Corresponding author: yangjm2007@lzu.cn

Received 19 May 2016; revised 9 September 2016; accepted 19 October 2016; posted 25 October 2016 (Doc. ID 266608); published 16 November 2016

A novel waveguide near to eye display (WGNED), with new in-coupling and propagation subsystems, is proposed for the first time, to our knowledge, to enlarge the vertical field-of-view (FOV) and the vertical size of the eye box. Two waveguides are stacked—one is for in-coupling and the other for out-coupling. A freeform prism is used to correct the aberrations. These components are combined to form the WGNED. We have simulated such a system; as a result, we show that it achieves a FOV of 30°horizontal (H) × 60°vertical (V) and an eye box of about 15 mm (H)× 12 mm (V). The modulation transfer function of the system is larger than 0.3 at 33 lp/mm and the distortion is smaller than 5%.

OCIS codes: (080.2740) Geometric optical design; (120.2040) Displays; (220.4610) Optical fabrication; (350.4600) Optical engineering; (330.7321) Vision coupled optical systems.

http://dx.doi.org/10.1364/OL.41.005426

In the past few years, near to eye displays (NEDs) have undergone rapid developments [1] with the release of a series of related commercial products, such as Microsoft HoloLens [2], Google Glasses [3], and Sony [4] and Nokia products [5]. NEDs can be classified as see-through, which is for augmented reality (AR) and immersive, which is for virtual reality (VR). For AR, see-through NEDs have the capability of superimposing a virtual image on the real-world scene; the virtual image and the real-world scene are seen simultaneously by the user [6]. There are various approaches to realize see-through systems such as using freeform optical prisms [7], projection systems [8,9], adaptive correcting optics [10], retinal scanning [11], reflective systems [12], hybrid reflective-refractive systems [13], and optical waveguides [14,15]. A very detailed review can be found in the literature [16,17]. The main requirements for such systems are compactness and lightness. However, it is a very difficult task to meet these criteria and keep high performance at the same time. The field-of-view (FOV) and the eye box are two of the key parameters to evaluate the optical performance of a NED. Each technology has its own constraints. According to the combiner type, NEDs can be separated into two families [16]: one is a free space combiner, which has no capability to expand pupil size; the other is a waveguide combiner, which can expand pupil size without increasing the Lagrange invariant. Therefore, the use of a waveguide can reduce the design difficulties and probably is the most promising approach. Waveguide technology can be classified into two types: geometrical waveguides and holographic waveguides. Both of them consist of an input-coupling and output-coupling subsystem. Lumus Company employs a reflective mirror for the input-coupling optics and an array of partially reflective mirrors (PRMA) for the output-coupling optics [18]. The PRMA is specially designed to have the right reflectance for different wavelengths and angles. Optinvent Company uses small cascaded mirrors as the out-coupling subsystem because the focus point of the eye is far from the mirrors [19]. Microsoft [2], Konica Minolta [20], Sony, and BAE Systems [21,22] have used diffractive optical elements (DOEs) or holographic optical elements (HOEs) to develop their WGNEDs. However, having a large FOV in both the horizontal and especially in the vertical direction is a difficult problem in WGNEDs. Horizontally, the FOV is limited by three parameters: the total internal reflection angle of the waveguide material, the expanded pupil size, and the distance between each reflection inside the waveguide. Normally, a horizontal FOV reaches around 20° inside the waveguide and 30° in air. As light from a pupil propagates divergently along the waveguide, vertical FOV is greatly dependent on the pupil size in this direction in order to reach the eye. It is about 9° with a pupil size of 8 mm from the equation proposed in [14]. In order to enlarge the FOV vertically, Amitai [14] proposed a two-dimensional aperture-expanding method using cascaded mirrors. Using the same concept, Eisen *et al.* [23] proposed a system with three holographic gratings for in-coupling light into the waveguide and expanding the eye box along orthogonal directions. Microsoft has also adopted this concept to develop HoloLens [2]. However, the FOV does not exceed 40°. Cheng *et al.* [15] proposed a two-pupil design by combining the freeform prism and the waveguide to address this problem. Using this method, Han *et al.* [24] designed a similar system with an 18°(H) × 24°(V) FOV. In this Letter, we introduce a new method—to the best of our knowledge—that can increase the vertical FOV to 60° and

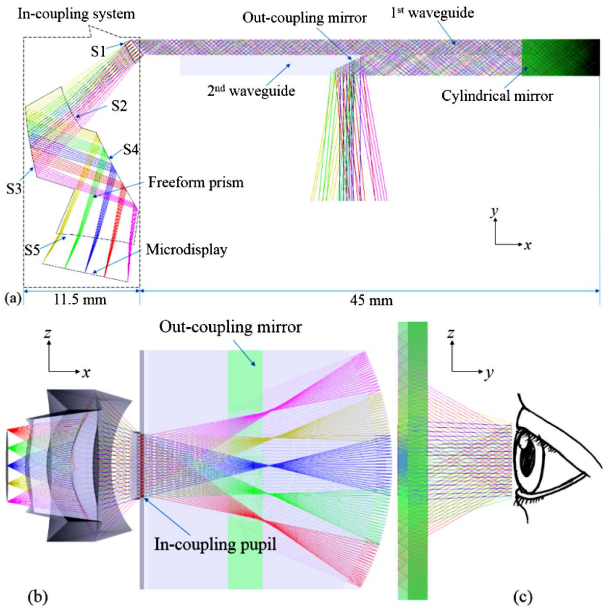

Fig. 1. Whole structure and optical path of the proposed system from different points of view: (a) *yx* view, (b) *zx* view, (c) *zy* view.

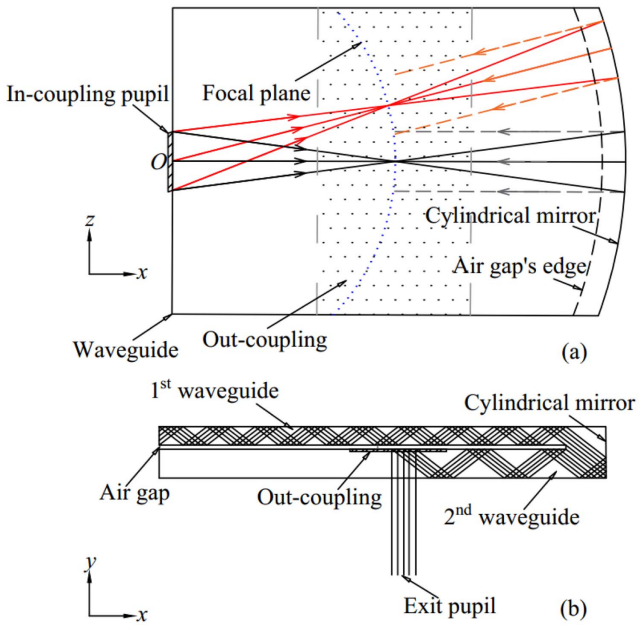

Fig. 2. Schematic for the designed system. (a) Ray path in *zx* plane. The dashed rays are the rays that are coupled into the second waveguide. (b) Ray path in *yx* plane. The air gap is magnified for clarity.

enlarge the vertical size of the eye box to 12 mm. Using cascaded mirrors as the Lumus waveguide type, the horizontal size of the eye box can be expanded to 15 mm. The total FOV is then 30°(H) × 60°(V) with a total eye box of 15 mm (H)× 12 mm (V), which is, to our knowledge, the largest FOV among the published WGNEDs.

Figure 1 shows the structure of the system and the ray path inside. Two waveguides are stacked up with a small air gap so that light can propagate inside the two waveguides independently. The light emitted by the micro-display is coupled into the first waveguide by the in-coupling subsystem. Light propagates inside the first waveguide until reaching a cylindrical mirror at the end of the waveguide. In the area near the mirror, the two waveguides are combined. Then, the light reflected by the cylindrical mirror is coupled into the second waveguide. Using an existing method such as a hologram or cascaded mirrors, the light is coupled out from the second waveguide. The in-coupling system consists of a prism with four different optical freeform surfaces (from S2 to S5) and a lens made of a freeform surface (S1) and a plane surface. This complex prism gives more freedom to correct aberrations. Moreover, it can be fabricated in one piece. As the FOV in the horizontal direction is limited to 30° in air, the total light section is small; as a consequence, S2 and S4 surfaces can be separated. The in-coupling pupil has a rectangular shape with a size of 1.9 mm (H) × 12 mm (V), which acts as a stop aperture and then greatly reduces the stray light. Pupil size is enlarged by adding vignetting along the *z* direction as shown in Figs. 1(b) and 1(c).

The center *O* of the in-coupling pupil, shown in Fig. 2(a), is the center of the cylindrical mirror and also the center of the cylindrical edge of the air gap. After the reflection, the chief ray of each field will go backward and converge to a point. The associated propagating length is the radius of the cylindrical mirror. The position of the eye should be near this point, so that each field can be seen as shown in Fig. 1(c).

The focal property of light after the in-coupling pupil is different in the *zx* plane and *yx* plane because of the cylindrical mirror shown in Fig. 2. Let *R* be the radius of curvature for the cylindrical mirror. In the case of paraxial approximation, rays converge to the focal plane of the cylindrical mirror, which is located at $R/2$ from the center in the *zx* plane as shown in Fig. 2(a). Then the rays are reflected by the cylindrical mirror and become a parallel beam that is coupled into the second waveguide. However, as the cylindrical mirror has no optical power in the *yx* plane, the light should be a parallel beam after the in-coupling pupil as shown in Fig. 2(b). To compensate for the large optical power caused by the cylindrical mirror, we use a freeform prism and a lens to correct aberrations in which all the surfaces are XY polynomials. The optical power in the *yx* plane is mainly given by the mirror S3 [Fig. 1(a)]. The advantage of this design is a large pupil size (12 mm) in the *z* direction with high image quality. Using the in-coupling system mentioned above, the beam then becomes parallel in both directions after the reflection from the cylindrical mirror. Finally, it is coupled out to the user's eye.

For coupling the light from the first to the second waveguide, the length *L* of the transition region (filled area with

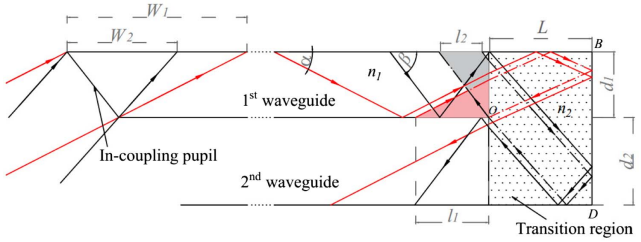

Fig. 3. Ray path of coupling from the first waveguide to the second waveguide.

points in Fig. 3) and the thickness of the second waveguide d_2 are interdependent; both are critical. As shown in Fig. 3, the red arrow lines correspond to the propagating field with a minimum tilt angle (α) and the black arrow lines correspond to the field with a maximum tilt angle (β). In the following, we call the minimum (resp. maximum) field, the field whose chief ray has the minimum (resp. maximum) tilt angle. As the air gap is very small, it is not represented in the figure. Let n_1 be the refractive index of the two waveguides and n_2 be the refractive index of the transition region. For each field, a part of the rays cannot be coupled into the second waveguide, for example, the chief ray of the maximum field reflected inside the gray area and the chief ray of the minimum field reflected inside the red area. These rays are reflected back to the first waveguide, which limits the coupling efficiency.

The side lengths of the filled area along the waveguide are l_1 for the minimum field and l_2 for the maximum field. They are given by

$$l_1 = \frac{2}{\tan(\alpha)}\left(d_1 - \frac{Ln_1\ \sin(\alpha)}{\sqrt{n_2^2 - n_1^2\sin^2(\alpha)}}\right), \tag{1}$$

$$l_2 = \frac{2}{\tan(\beta)}\left(\frac{Ln_1\ \sin(\beta)}{\sqrt{n_2^2 - n_1^2\sin^2(\beta)}} - d_2\right). \tag{2}$$

In the design process we first fix d_1. Lengths l_1 and l_2 should be zero if all the light from the first waveguide is coupled into the second waveguide. The limit value of the length L of the transition region is obtained by setting $l_1 = 0$:

$$L = \frac{d_1\sqrt{n_2^2 - n_1^2\sin^2(\alpha)}}{n_1\ \sin(\alpha)}. \tag{3}$$

The minimum thickness of the second waveguide d_2 is obtained when $l_2 = 0$:

$$d_2 = \frac{Ln_1\ \sin(\beta)}{\sqrt{n_2^2 - n_1^2\sin^2(\beta)}}. \tag{4}$$

Combining Eqs. (3) and (4) we get the minimum value for d_2:

$$d_{2\ \min} = \frac{d_1\ \sin(\beta)\sqrt{n_2^2 - n_1^2\sin^2(\alpha)}}{\sin(\alpha)\sqrt{n_2^2 - n_1^2\sin^2(\beta)}}. \tag{5}$$

The relationship between d_2 with respect to other parameters can be found in [25]. It would be interesting to reduce the thickness of the second waveguide to decrease the weight and size. This introduces some additional coupling losses. In the following, the transition region and the two waveguides are assumed to be made with the same material and the thicknesses verify $d_1 < d_2$ in order to avoid high losses. By setting $l_1 = l_2 = 0$, we get the following critical values for α and β, respectively:

$$\alpha' = \arctan\left(\frac{d_1}{L}\right), \tag{6}$$

$$\beta' = \arctan\left(\frac{d_2}{L}\right). \tag{7}$$

Three situations occur for the coupling from the first waveguide to the second. In the first one, the field angle lies inside the interval $[\alpha, \alpha']$ and l_1, the side length of the red area along the waveguide, is given by Eq. (1). In the second situation, when the field angle lies inside the interval $[\alpha', \beta']$, there is no coupling loss. When the field angle lies inside the interval $[\beta', \beta]$, l_2, the side length of the shaded area along the waveguide, is determined by Eq. (2). In order to calculate the length of the transition region, as the first case we can set $l_1 = l_2$, then we obtain

$$L = \frac{d_1\ \cot(\alpha) + d_2\ \cot(\beta)}{2}. \tag{8}$$

In Fig. 3, W_1 and W_2 are the lengths of the waveguide covered by the minimum and the maximum fields. The coupling efficiencies are different if $l_1 = l_2$. To obtain the same coupling efficiency, we need

$$\frac{l_1}{W_1} = \frac{l_2}{W_2}. \tag{9}$$

In this second case, the length of the transition region is given by

$$L = \frac{W_2 d_1\ \cot(\alpha) + W_1 d_2\ \cot(\beta)}{W_1 + W_2}. \tag{10}$$

As an example, using PMMA ($n = 1.49$), if we set $d_1 = 1.5$ mm and $d_2 = 2$ mm, we obtain the different parameters shown in Table 1 for the two cases.

The maximum value of $\beta' - \alpha'$, which represents the range without loss, is 8.2°. The value of $\beta' - \alpha'$ for the two cases is 7.9° and 8°, respectively. The differences from the maximum value are very small. The second case offers a better coupling uniformity. Actual efficiency for a specific field could be higher depending on the amount of light falling into the filled regions (Fig. 3). The efficiency for the vertical fields is uniform because the center of the in-coupling pupil O is also the center of the cylindrical mirror and the center of the cylindrical edge of the air gap [Fig. 2(a)]. Therefore, each vertical field has the same coupling efficiency.

We have designed a system with the presented method and the parameters described above using Zemax. A 0.61 in. (1.5494 cm) OLED microdisplay with 852 × 600 pixels is used as the image source. The pixel size is 15 μm, which corresponds to a Nyquist frequency of 33 lp/mm. The horizontal FOV is set to 20°. The vertical FOV is 60°. The modulation transfer function (MTF) of the 12 object fields is plotted in Fig. 4(a). They are evaluated with a full rectangular pupil size of 1.9 mm (H) × 12 mm (V). All the values are above 0.3 at 33 lp/mm, which is sufficient for a visual system. The vertical

Table 1. Value of the Parameters in Two Cases (Case 1: the Lengths l_1 and l_2 are Equal; Case 2: the Same Coupling Efficiency)

Parameters	Case 1	Case 2
L (mm)	2.3	2.2
α (°)	28	28
β (°)	48	48
α' (°)	33.0	34.3
β' (°)	40.9	42.3
l_1 (mm)	1.02	1.25
l_2 (mm)	1.02	0.8
Coupling efficiency for the minimum field (%)	74.3	68.6
Coupling efficiency for the maximum field (%)	59.7	68.6

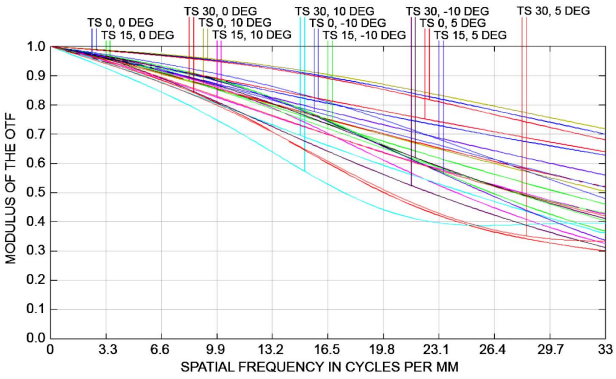

Fig. 4. MTF curves of the system with the 12 evaluated fields in object angle mode. *T* and *S* represent the tangential and sagittal MTFs of each field separately.

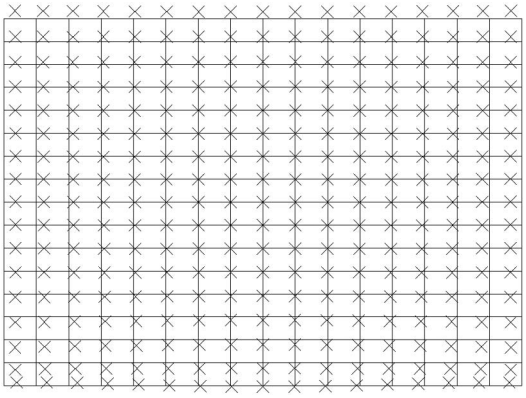

Fig. 5. Grid distortion of the system.

Table 2. Performance of the System

Parameters	Value
Field-of-view (H × V)	30° × 60°
In-coupling pupil (H × V mm)	1.9 × 12
Eye box (H × V mm)	≈15 × 12
System MTF	>0.3 at 33 lp/mm
Distortion	<4.5%
Monocular weight (g)	11
Magnification ratio (V/H)	1.6

and horizontal magnifications are different and in a ratio of 1.6. Figure 5 shows the grid distortion of the system with respect to the central field. The maximum distortion is 4.5% at the corner.

The performance of the system is summarized in Table 2. To estimate the value of the eye box in the horizontal direction, a Lumus-waveguide-type out-coupling system has been used. The weight in Table 2 takes into account all the optical components.

Figures 4 and 5 show that a good image quality can be expected for the whole FOV. A foreseen difficulty comes from fabrication and testing since the freeform prism has a complex shape. The current way to realize it is plastic molding injection. A prototype fabrication is still a high-cost operation.

In conclusion, we proposed a new polychromatic compact WNED system design by combining a freeform prism and two waveguides. The two waveguides have a cylindrical edge and are separated by a small air gap. The coupling from the first waveguide to the second has been investigated and optimized. As a result, we obtain an increased FOV of 30°(H) × 60°(V) and a very large eye box of about 15 mm (H) × 12 mm (V) allowing large eye movements.

Funding. SATT Conectus Alsace (project I15-061); China Scholarship Council (CSC).

Acknowledgment. Portions of this work were presented at the SPIE Photonics Europe Conference in 2016, Photonics and Digital Technologies for Imaging Applications IV, 989605.

REFERENCES

1. J. Rolland and O. Cakmakci, Opt. Photon. News **20**(4), 20 (2009).
2. A. Travis, "Wide field-of-view virtual image projector," U.S. patent 20,130,021,392 A1 (January 24, 2013).
3. M. J. Heinrich and M. I. Olsson, "Wearable display device," U.S. patent D659,741 (May 15, 2012).
4. H. Mukawa, K. Akutsu, I. Matsumura, S. Nakano, T. Yoshida, M. Kuwahara, and K. Aiki, J. Soc. Inf. Disp. **17**, 185 (2009).
5. P. Äyräs, P. Saarikko, and T. Levola, J. Soc. Inf. Disp. **17**, 659 (2009).
6. R. Azuma, Y. Baillot, R. Behringer, S. Feiner, S. Julier, and B. Macintyre, IEEE Comput. Graph. Appl. **21**, 34 (2001).
7. S. Yamazaki, K. Inoguchi, Y. Saito, H. Morishima, and N. Taniguchi, Proc. SPIE **3639**, 453 (1999).
8. H. Hua, A. Girardot, C. Gao, and J. P. Rolland, Appl. Opt. **39**, 3814 (2000).
9. R. Martins, V. Shaoulov, Y. Ha, and J. P. Rolland, Opt. Express **15**, 14530 (2007).
10. M. Beuret, P. Twardowski, and J. Fontaine, Opt. Express **19**, 19688 (2011).
11. M. M. Bayer, Proc. SPIE **4711**, 202 (2002).
12. A. Bauer and J. P. Rolland, Opt. Express **22**, 13155 (2014).
13. J. Yang, W. Liu, W. Lv, D. Zhang, F. He, Z. Wei, and Y. Kang, Opt. Lett. **38**, 2035 (2013).
14. Y. Amitai, in *SID International Symposium Digest of Technical Papers* (2005), Vol. **36**, p. 360.
15. D. Cheng, Y. Wang, C. Xu, W. Song, and G. Jin, Opt. Express **22**, 20705 (2014).
16. B. Kress and T. Starner, Proc. SPIE **8720**, 87200A (2013).
17. O. Cakmakci and J. Rolland, J. Disp. Technol. **2**, 199 (2006).
18. Y. Amitai, "Substrate-guided optical devices," U.S. patent 7,672,055 B2 (March 2, 2010).
19. G. Dubroca, P. Benot, K. Sarayeddine, and X. Hugel, "Monolithic low cost plastic guide for full color see-through personal video glasses," in *Proceedings of International Display Workshops (IDW)*, Fukuoka, Japan, 2010, Vol. **2**, p. 1355.
20. I. Kasai, Y. Tanijiri, E. Takeshi, and U. Hiroaki, Opt. Rev. **8**, 241 (2001).
21. I. K. Wilmington and M. S. Valera, in *SID Symposium Digest of Technical Papers* (2013), Vol. **44**, pp. 278–280.
22. A. A. Cameron, Proc. SPIE **383**, 83830E (2012).
23. L. Eisen, M. Meyklyar, M. Golub, A. A. Friesem, I. Gurwich, and V. Weiss, Appl. Opt. **45**, 4005 (2006).
24. J. Han, J. Liu, X. Yao, and Y. Wang, Opt. Express **23**, 3534 (2015).
25. J. Yang, P. Gérard, P. Twardowski, and J. Fontaine, Proc. SPIE **9896**, 989605 (2016).